Proceedings of CREEP8
Eighth International Conference on Creep and Fatigue at Elevated Temperatures
July 22-26, 2007, San Antonio, Texas

CREEP2007-26019

TEMPERATURE AND ORIENTATION DEPENDENCE OF CREEP DAMAGE OF TWO NI-BASE SUPERALLOYS

Ali P. Gordon*
Department of Mechanical, Materials, Aerospace Engineering, University of Central Florida
Orlando, FL 32816-2450

Sameer Khan
Gas Turbine Engineering, Siemens-Westinghouse Power Corporation
Orlando, FL 32826-2399

David W. Nicholson
Department of Mechanical, Materials, Aerospace Engineering, University of Central Florida
Orlando, FL 32816-2450

ABSTRACT

Both polycrystalline (PC) and directionally-solidified (DS) Ni-base superalloys are commonly applied as turbine materials to primarily withstand creep conditions manifested in either marine-, air- or land-based gas turbines components. The thrust for increased efficiency of these systems, however, translates into the need for these materials to exhibit considerable strength and temperature resistance. This is critical for engine parts that are subjected to high temperature and stress conditions sustained for long periods of time, such as blades, vanes, and combustion pieces. Accurate estimates of stress and deformation histories at notches, curves, and other critical locations of such components are crucial for life prediction and calculation of service intervals. In the current study, the classical Kachanov-Rabotnov model for tertiary creep damage is implemented in a general-purpose finite element analysis (FEA) software. Creep deformation and rupture experiments on samples from two representative Ni-base superalloys (PC and DS) tested at temperatures between 649 and 982°C and two orientations (longitudinally- and transversely-oriented for the DS case only) are applied to extend this damage formulation. The damage model coefficients corresponding to secondary and tertiary creep constants are characterized for temperature and orientation dependence. This updated formulation can be implemented for modeling full-scale parts containing temperature distributions.

INTRODUCTION

Both polycrystalline (PC) nickel-chromium-cobalt-molybdenum alloys (similar to wrought HAYNES® 230) and directionally-solidified (DS) Ni_3Al superalloys (similar to cast DS René 80) are commonly applied in turbine components designed to transport super-heated, high pressure gases through power generation equipment. Each class of materials is solid-solution strengthened with chemical compositions imparting exceptional combinations of high-temperature strength and oxidation resistance. One characteristic of both of these materials is the high strength levels they maintain at elevated temperatures. The resistance of the alloys to high-temperature corrosion enhances the usefulness of its strength. Although they are suitable below 1000°C, they both display high levels of creep-rupture strength, even at temperatures of 982°C (1800°F). These traits, combined with good resistance to oxidizing and carburizing atmospheres, make the alloys especially suitable for long-term, high-stress use at elevated temperatures. For example, wrought NiCr alloys have good combinations of metallurgical stability, strength, and oxidation resistance at high temperatures. These alloys are also readily formed and welded by conventional techniques for use in transition lines, exhaust ducting, etc.

The DS materials have dual-phase γ-γ′ microstructures that have been optimized to maximize creep and fatigue resistance. The material contains matrix and precipitate phases, as shown in Fig. 1.a. Grains are columnar and aligned along the primary stress axis of the component such as a turbine blade axis. Dissimilar to the PC materials discussed above, DS superalloys can be assumed as transversely isotropic. Two orientations commonly considered for characterizing the uniaxial behavior of DS materials are those in which grains are longitudinally-oriented (L-oriented) and transversely-oriented (T-oriented), as shown in Fig. 1.b. It should be noted that due to fact that more grains are expected to be contained in the cross-section of a T-oriented sample as opposed to the L-oriented specimen, the T-oriented case is expected to have behavior similar to a PC material Ni-base superalloy. The grains along the L- and T-orientations of the DS material are shown in Fig. 2.

* Corresponding Author. Tel.: +1-407-823-4986; Fax: +1-407-823-0208;
E-mail: apgordon@mail.ucf.edu.

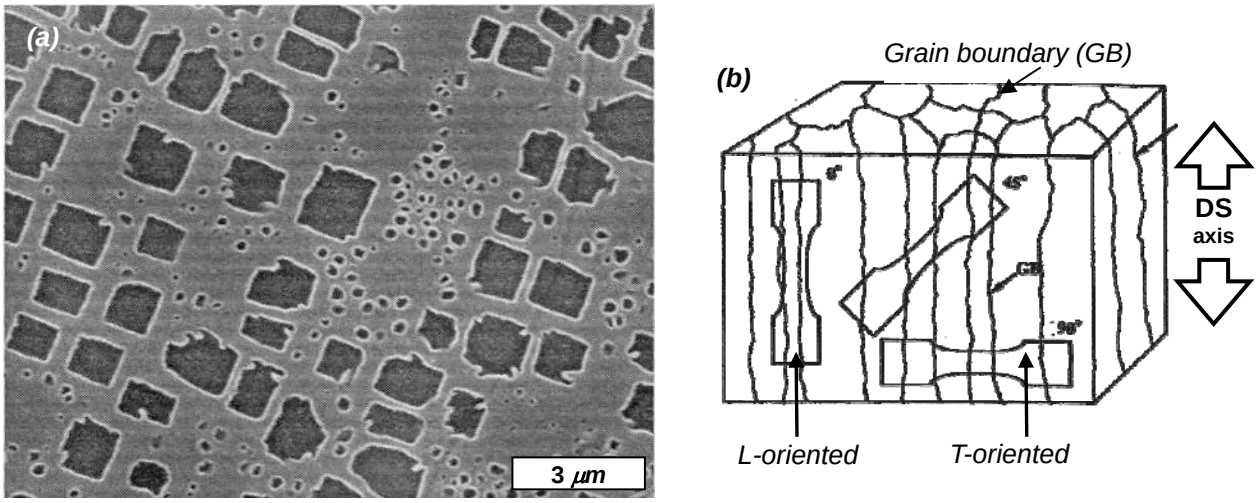

Figure 1: *(a) Image of the matrix and (course and fine) precipitate phases, and (b) sketch of grain boundaries and sectioning convention for a DS Ni-base superalloy.*

Service conditions for these components are designed using practical experience along with finite element modeling. Despite the strengths of these materials, the combinations of temperature and stress gradients, corrosive conditions, and complex duty cycling facilitate the onset of a myriad of damage mechanisms which lead to crack initiation and subsequent rupture. Calculations of remaining creep rupture life estimates are also developed using experience and secondary creep modeling. Because this strategy lacks consideration of the temperature-dependent, strain-softening behavior (i.e., tertiary creep), both strain history and life estimates have limited accuracy. By incorporating creep damage, a substantial improvement in life prediction is achievable. Creep deformation and rupture data are used to implement a constitutive model in a general purpose finite element analysis code. Experimental results are then compared with numerical calculations.

TERTIARY CREEP DAMAGE

A method has been established for modeling tertiary creep at high temperatures. This method is based on the Norton power law for secondary creep, i.e.,

$$\dot{\varepsilon}_{cr} = A\bar{\sigma}^n, \tag{1}$$

where A and n are the creep strain coefficient and exponent, respectively, and $\bar{\sigma}$ is the von Mises effective stress. The coefficient A exhibits Arrhenian temperature-dependence, e.g.

$$A = B\exp\left(-\frac{Q_{cr}}{RT}\right). \tag{2}$$

Here Q_{cr} is the activation energy for creep deformation, and T is the temperature measured in Kelvin. The term R is the universal gas constant. Both A and its temperature-independent counterpart, the coefficient B, have units $MPa^{-n}hr^{-1}$. It should be noted that the exponent n may also exhibit temperature-dependence.

During the transition from secondary to tertiary creep, stresses in the vicinity of voids and microcracks along grain boundaries of polycrystalline materials are amplified. In DS materials, tertiary creep is facilitated by microcracking at inclusion particles that are abundantly found in interdendritic regions. The stress concentration due to local reduction of cross-sectional area is the phenomenological basis of the Kachanov-Rabotnov damage variable, ω, that is coupled with the creep strain rate and has a stress-dependent evolution, i.e.,

$$\begin{aligned}\dot{\varepsilon}_{cr} &= \dot{\varepsilon}_{cr}\left(\boldsymbol{\sigma}, T, \omega, \ldots\right)\\ \dot{\omega} &= \dot{\omega}\left(\boldsymbol{\sigma}, T, \omega, \ldots\right)\end{aligned}. \tag{3}$$

A straightforward formulation implies that the damage variable is the net reduction in cross-sectional area due to the presence of defects such as voids and/or cracks, e.g.

$$\bar{\sigma}_{net} = \frac{\bar{\sigma}}{1-\omega}. \tag{4}$$

An essential feature of damage required for application of continuum damage mechanics concepts is a continuous distribution of damage. Generally, micro-defect interaction (in terms of stress fields, strain fields, driving forces) is relatively weak until impingement or coalescence is imminent. By substituting Eq. (4) into (1), the steady-state creep strain is expressed as a modified secondary creep rate

$$\dot{\varepsilon}_{cr} = A\left(\frac{\bar{\sigma}}{1-\omega}\right)^n. \tag{5}$$

The isotropic damage variable, ω, is scalar-valued from 0 for an initial state (e.g. undamaged) to 1 at final state (e.g. completely ruptured). Its evolution was given by Rabotnov [1] as

$$\dot{\omega} = \frac{M\sigma^{\chi}}{(1-\omega)^{\phi}}, \tag{6}$$

where M is the creep damage coefficient having units of $MPa^{-\chi}hr^{-1}$. In an earlier study, Kachanov [2] developed a

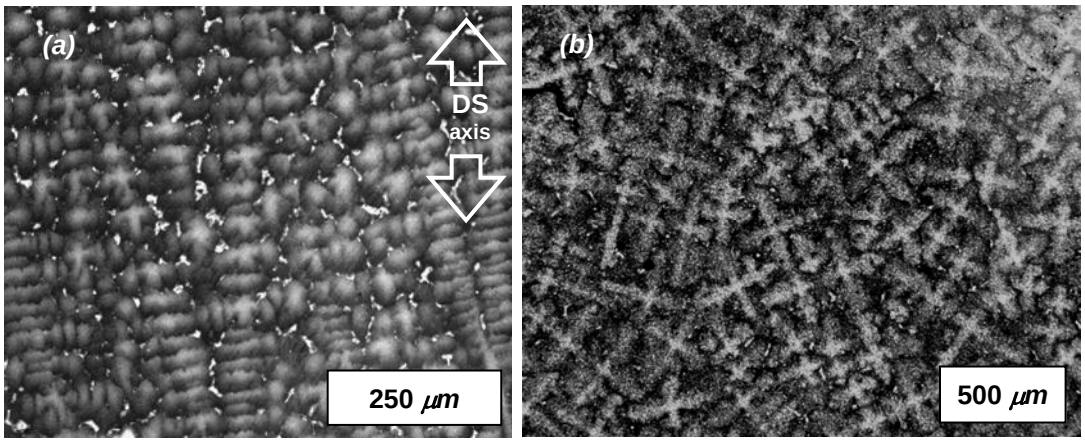

Figure 2: *Grain structures of sections (a) parallel (e.g. L-oriented) and (b) perpendicular (T-oriented) to the primary stress axis of directionally-solidified Ni-base specimens.*

similar formulation with the exception that the creep damage exponents, χ and ϕ were equivalent. Later investigations have extended this damage evolution description to account for anisotropic damage resulting from multiaxial states of stress [3]. In these cases, damage is described by a second-rank tensor.

Equations (5) and (6) can be applied to model the gradual reduction of load carrying capability (e.g. secondary through tertiary creep). Since ω characterizes the microstructural evolution of the material and is dependent on stress and temperature, the damage variable is an internal state variable (ISV). Clearly, the coupled evolution equations reduce to secondary creep when $M = 0$.

This formulation has been used in a variety of studies of turbine and rotor materials. The constants A, n, M, χ, and ϕ are considered material properties. For example, in Waspaloy at 700°C, $A = 9.23\times10^{-34}$ $MPa^{-n}hr^{-1}$, $n = 10.65$, $M = 1.18\times10^{-25}$ $MPa^{-\chi}hr^{-1}$, $\chi = 8.13$, and $\phi = 13.0$ [4]. For stainless steel at 650°C, $A = 2.13\times10^{-13}$ $MPa^{-n}hr^{-1}$, n =3.5, $M = 9.0\times10^{-10}$ $MPa^{-\chi}hr^{-1}$, and $\chi = \phi = 2.8$ [5]. In these previous studies, isothermal and constant stress conditions were applied. It should be noted that no rule for the temperature dependence of the tertiary creep constants has been established. Additionally, other formulations for modeling tertiary creep are available (e.g. theta-projection method [6]); however, the current method is the most widely used.

Creep deformation and rupture experiments described in previous test programs and available in literature [7,8] were evaluated using the tertiary creep damage model. In both PC and DS cases, tests were conducted according to an ASTM standard E-139 [9] at 649, 760, 871, and 982°C on samples incised from cast and wrought slabs. It has been demonstrated from this variety of creep deformation and rupture experiments that the subject DS material exhibits primary, secondary, and tertiary creep strain depending on the combination of test temperature and stress, as shown in Fig. 3 [8]. This is also the case for the PC material.

Based on these strain histories, the deformation mechanisms can be inferred from investigations that complemented mechanical experimentation with microscopic analysis [10,11]. Deformation at 649°C is mostly due to elastic strain, along with primary and secondary creep. During primary creep, the strain rate, which is initially high, decreases significantly. This transient phenomenon is due to the ease at which dislocations can occur upon initial loading and the saturation of the dislocation density which inhibits continued creep deformation. Secondary creep arises due to the nucleation of grain boundary (GB) cavities and grain boundary sliding. Tertiary creep behavior was not observed in these cases. At higher temperatures (760°C and above), deformation is dominated by tertiary creep facilitated by the coalescence of grain boundary voids into microcracks. Primary creep was also observed, but its contribution to the overall deformation was negligible compared to that of tertiary creep.

Depending on the experimental configurations, creep tests can take a long time to perform. The Larson-Miller parameter, e.g. LMP, [12] has been established to aid in the prediction of creep rates or creep rupture times. It is important to note that this parameter assumes that the majority of life is used up during steady state creep (e.g. $\varepsilon \approx \dot{\varepsilon} \cdot t_r$), e.g.,

$$LMP = T\left(C + \log t_r\right)/1000 \tag{7}$$

where t_r is the time to rupture (in hours) and C is constant (in log hours). The temperature, T, is measured in Kelvin (K). The LMP is typically used as a design parameter against creep rupture.

Creep rupture data from experiments on the L- and T-oriented DS are compared with those of the PC material via a plot of stress versus LMP, as show in Fig. 4. For a given stress, LMP data of the L-oriented DS material lie slightly to the right of data generated for the T-oriented and PC materials. This

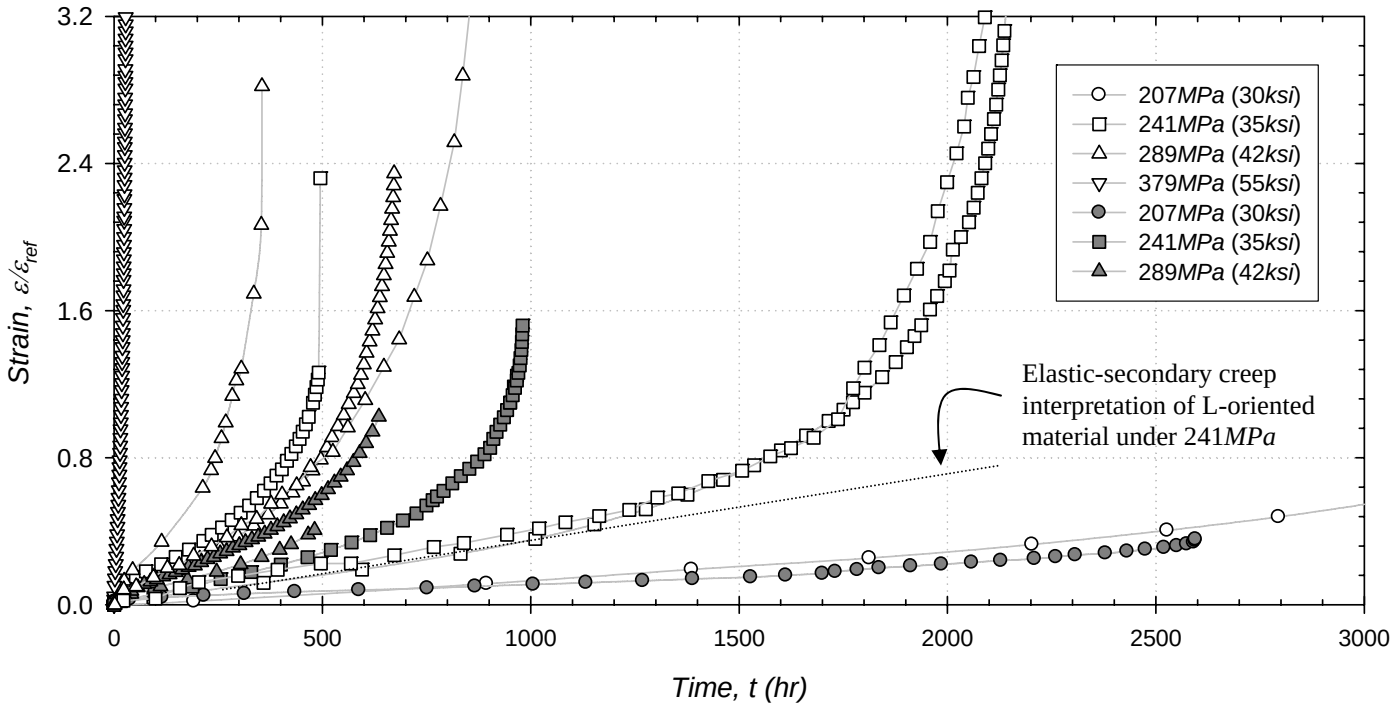

Figure 3: *Creep deformation and rupture of a L-oriented (unfilled symbols) and T-oriented (filled symbols) directionally-solidified Ni-base superalloy at 871°C.*

small difference corresponds to an increase of resistance to creep rupture of at least 25°C (45°F). Such comparisons may also be achieved with creep rupture results base on other Ni-base isotropic PC materials [13-17], and DS materials [18-20].

NUMERICAL METHODLOGY

The constitutive model described in Eqs. (5) and (6) has been implemented in a general purpose finite element analysis software in order to determine the constants for the constitutive model used in the secondary-tertiary creep formulation. Both equations were written into a FORTRAN subroutine in the form suitable to the FEA program. The subroutine is incorporated with an implicit integration algorithm. This backward Euler integration algorithm is more robust and accurate for long time periods, when viscoplastic/creep behavior of materials is significant. Using this method, uniaxial creep law has been specified and is generalized to the multiaxial state by the general time-dependent viscoplastic material formulation. This formulation allows for the update of the internal state variable, ω. Initially, $\omega = 0$ and during loading, ω increases. To prevent the singularity that is caused by rupture (e.g. $\omega = 1$), the damage is restricted to a maximum of 0.90. This model can be coupled with time-independent and dependent plasticity models with ease.

A material model has been used to simulate the stress/temperature loading conditions of a series of uniaxial creep and rupture experiments. A single, solid, three-dimensional, 8-noded element was used, and the appropriate initial and boundary conditions were applied to numerically simulate uniaxial creep deformation. Temperatures of 649, 760, 871, and 982°C were applied since samples exhibited tertiary creep deformation. At least on stress level was applied for each temperature.

Coupling the Norton power law for secondary creep with the Kachanov-Rabotnov formulation for tertiary creep allows the finite element model to display a strain history that is in close proximity to experimental results. The secondary creep constants (e.g. A and n) were analytically evaluated directly from the available creep deformation data. Consequently, B and Q_{cr} were approximated via a regression analysis of Eq. (2).

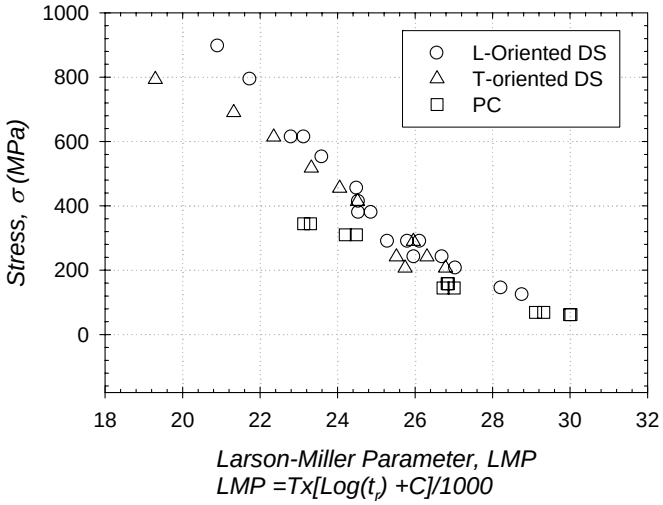

Figure 4: *Larson-Miller Parameter for creep rupture of several Ni-base superalloys.*

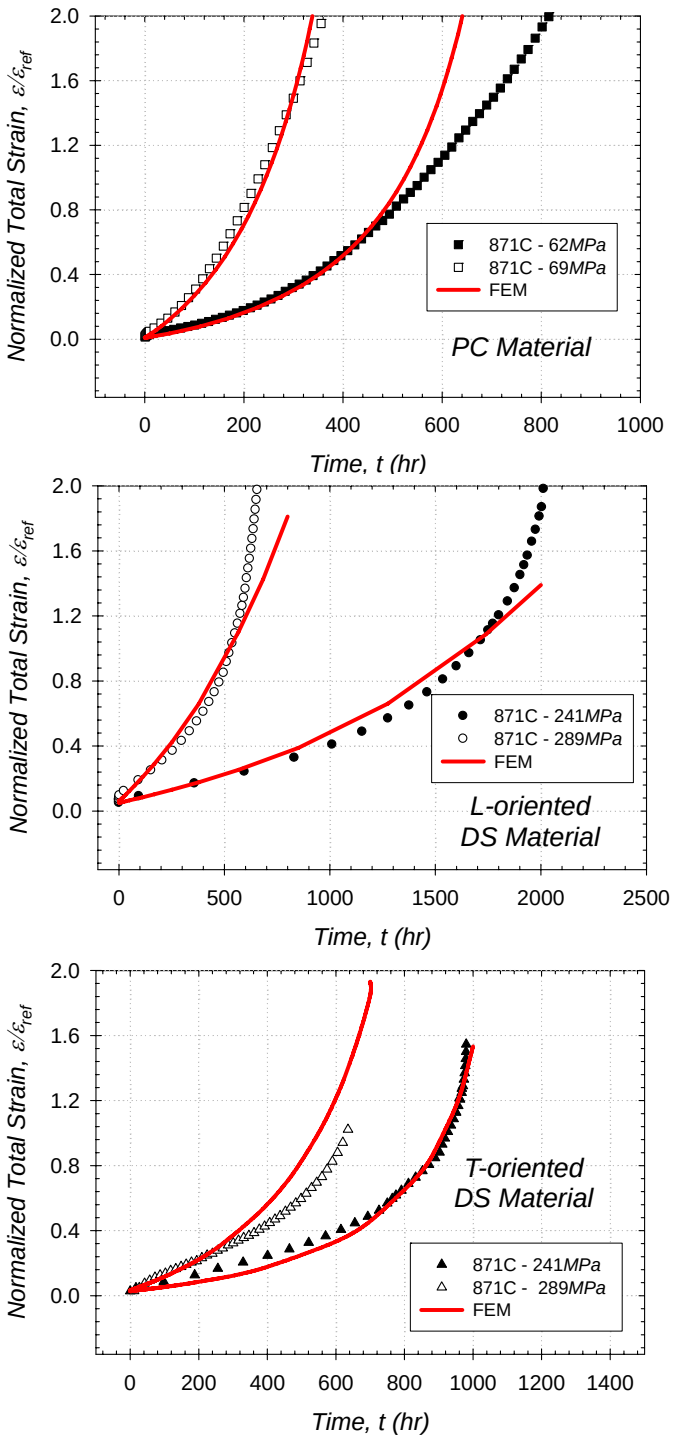

Figure 5: *Comparison of experimental and numerically simulated creep deformation vary Ni-base alloys 871°C (1600°F).*

The tertiary creep constants (e.g. M, χ, and ϕ) were determined for each temperature by an automated iterative trial and error. Since only uniaxial data are available, χ and ϕ were taken to be equivalent and non-varying with respect to temperature. Tertiary creep constants were optimized for every combination of temperature and stress.

RESULTS

Comparisons of the simulated creep deformation responses are shown Fig. 5 for 871°C. The strain histories simulated with the Norton-Rabotnov formulation correlate well with the analogous experimentally-obtained $\varepsilon(t)$. In all cases, the trajectory of each of the correlated creep curves nearly matched the corresponding experimental curve.

A goal of the study was to provide a uniaxial creep deformation formulation that was capable of matching the material response up to 5% of the creep strain determined from experiments; as such, simulations were carried out to 5% creep strain. The time required for each experimentally-tested specimen to deform to 5% is denoted by $t_{\varepsilon_{cr}=5\%}$. It should be noted that in application components exhibiting strains exceeding 5% are typically replaced or repaired. Each of the simulations was, therefore, carried out from an undamaged state (e.g. $\omega = 0$) to a creep deformation of beyond 5%.

For each of the temperatures at and above 760°C the coupled Norton-Rabotnov formulation predicts a deformation that is at least approximately 3.5 times larger than that of elastic and secondary creep modeling alone, as depicted in Fig. 3.

Given the secondary creep constants, all of the creep curves could be generated by varying M, χ, and ϕ. The creep damage rate coefficient, M, displays temperature dependence; however, the temperature dependence of the damage rate exponents χ and ϕ is saved for a future study.

Based on the experiments, the temperature dependence for each of the constants was analytically represented. The elastic modulus of the materials can be written as a 3rd order polynomial, e.g.

$$E(T) = E_3T^3 + E_2T^2 + E_1T + E_0, \tag{8}$$

where E_0, E_1, E_2, and E_3 are constants used to fit the tensile data for the PC and DS materials, as shown in Fig. 6.a. In Eq. (8), T is measured in degrees Kelvin. In a similar manner, regression analyses were performed to model the temperature dependence of the secondary creep and creep damage constants. The secondary creep coefficient was determined using the Arrhenius relation in Eq. (2), where B and Q_{cr} are each independent of temperature. The secondary creep exponent was related by a polynomial function (Fig. 8.c.), e.g.

$$n(T) = \left\langle n_3T^3 + n_2T^2 + n_1T + n_0 \right\rangle, \tag{9}$$

where T is measured in Kelvin. The McCauley brackets are used in this case so that n is always non-negative. The creep damage coefficient is expressed as a 2-parameter exponential power law function (Fig. 6.d.), e.g.

$$M(T) = M_1 \exp(M_0T). \tag{10}$$

Here M_1 and M_0 are constants. Equation (6) is modified to incorporate temperature dependence, i.e.

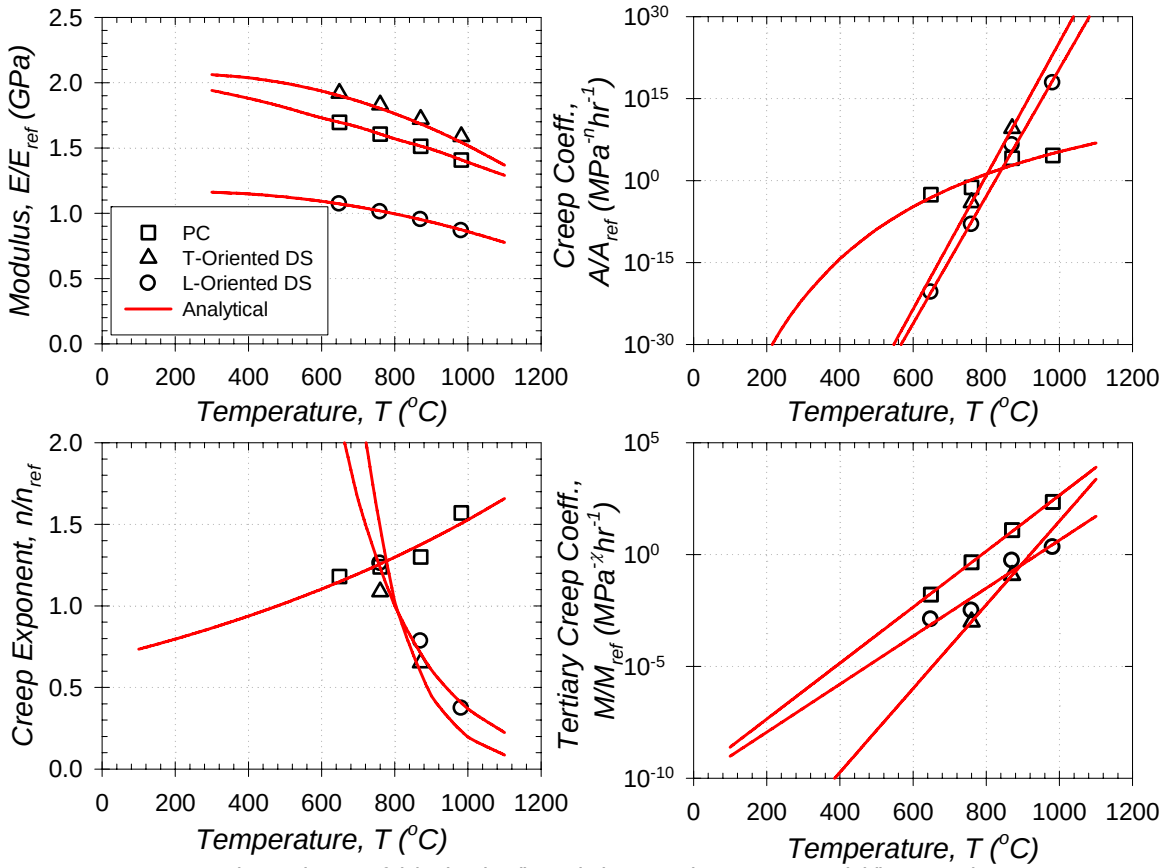

Figure 6: *Temperature dependence of (a) elastic, (b and c) secondary creep, and (d) creep damage constants of various Ni-base superalloys.*

$$\dot{\omega} = \frac{M_1 \sigma^{\chi} \exp\left(M_0 T\right)}{\left(1-\omega\right)^{\phi}}, \tag{11}$$

The fits of Eqs. (2) and (8) through (10) are compared with experimental data in Fig. 6. Results show that the temperature dependence of the elastic modulus for each material generally decreases with increasing temperature. The trends for the secondary creep constants (creep coefficient, *A*, and exponent, *n*) differed for PC and DS materials, although the L-oriented and T-oriented regressions resembled each other. This is attributed to the fact that the grain sizes and shapes of the materials are generally dissimilar.

The variation of the tertiary creep coefficients exhibited similar trends with respect to time, as shown in Fig. 6d. Of the three materials and temperature ranges considered, *M* was largest for all cases for the PC material compared to either orientation of the DS materials. This indicates that the PC material is the most susceptible to undergoing tertiary creep. Above temperatures of 982°C, the trend of *M* with temperature for the T-oriented DS material is likely to exhibit tertiary creep similar to a PC material.

The Larson-Miller Parameter was calculated from strain histories simulated via finite element modeling. The time in which the creep strain reached 5% (e.g. $t_{\varepsilon_{cr}=5\%}$) was used in place of the rupture time, t_r, e.g.

$$LMP_{\varepsilon_{cr}=5\%} = T\left(C + \log t_{\varepsilon_{cr}=5\%}\right)\Big/1000\,. \tag{12}$$

The LMP values were computed for each of the materials at a variety of temperature (649 through 982°C) and stress combinations. These points were curve fit using a 3rd order polynomial. For example, for the L-oriented DS material, the relationship was determined as follows:

$$\sigma = 0.23\left(LMP_{\varepsilon_{cr}=5\%}\right)^3 + 16.21\left(LMP_{\varepsilon_{cr}=5\%}\right)^2 - 269.12\left(LMP_{\varepsilon_{cr}=5\%}\right) + 581.93 \tag{12}$$

Here, stress has units of *MPa*. This curve along with two corresponding to the PC material and T-oriented DS material is shown in Fig. 7.a.

Comparisons between the experimental and the numerically simulated $LMP_{\varepsilon_{cr}=5\%}$ is shown in Fig. 7.b. A variety of temperature and stress levels were used for each material. Regardless of the case, the experimental and simulated values of $LMP_{\varepsilon_{cr}=5\%}$ are within error bands of 5%. In most cases, the relative error is less than 1%.

CONCLUSIONS

The materials used in gas turbine components fail by a number of physical mechanisms and combinations thereof. The focus of this investigation was modeling the creep deformation of materials used to fabricate turbine parts that exhibit strain softening at high temperatures (above 649°C). Creep cavitation, void coalesce along and within the

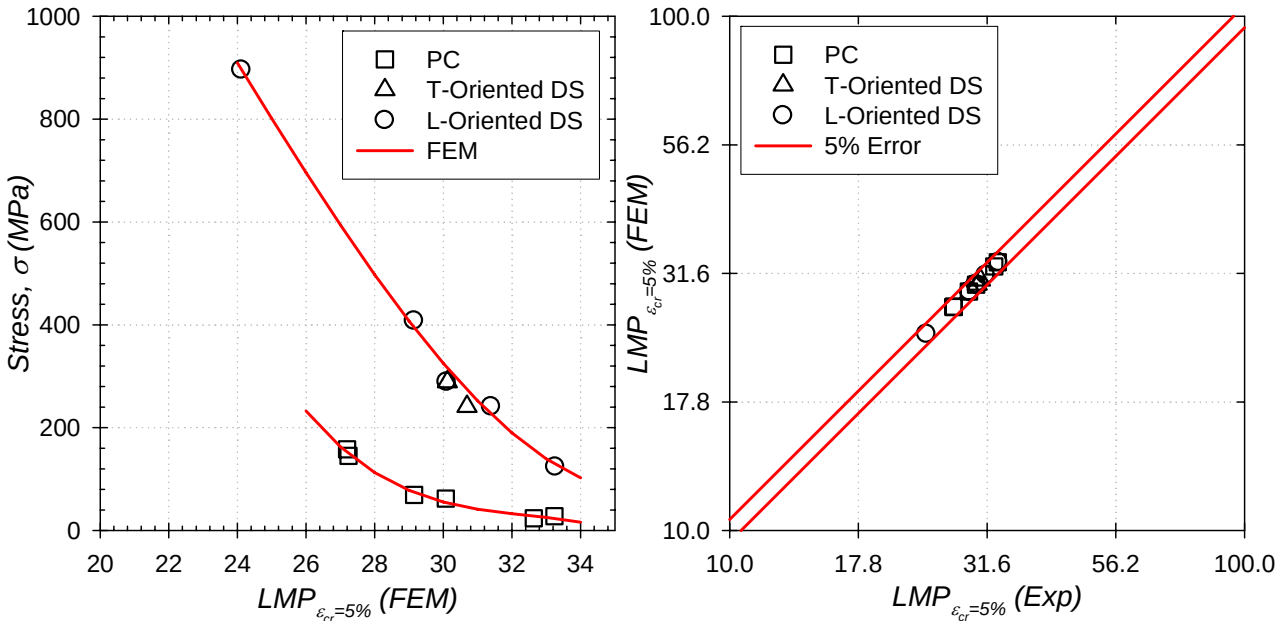

Figure 7: *Simulated (material model) Larson-Miller Parameter (LMP) for time to 5% creep strain (a) plotted versus stress and (b) plotted versus experiments.*

boundaries of grains leads to area-reduction transverse to the applied loading axis. This leads to gradual loss of stress-carrying ability. The Kachanov-Rabotnov-type creep damage formulation was used to account for this behavior found in creep deformation and rupture experiments carried out on the three distinct Ni-base materials.

To account for temperature dependence, phenomenological models were developed for several mechanical properties. The damage formulation was modified and directly implemented into the constitutive model routine [e.g. ABAQUS User-defined Material (UMAT)] so that predictions of creep deformation could be made through a range of temperatures. The correlated curves show excellent agreement with trends from creep deformation experiments.

The grain orientation dependence of the scalar-valued damage parameter model was explored by considering the creep deformation histories of an L- and T-oriented DS material. The variation of the parameters between these two orientations is saved for a later study.

ACKNOWLEDGMENTS

The authors are thankful for the assistance from Maria Duarte and Fred Shamieh in conducting finite element analyses. Ali P. Gordon is grateful for the support of a NSF-FACES grant.

REFERENCES

[1] Rabotnov, Y. N., (1969). “Creep Problems in Structural Members” North Holland, Amsterdam.

[2] Kachanov, L. M. (1958). "Time to Rupture Process Under Creep Conditions." *Izv. Akad. Nank.* 8: 26-31.

[3] Murakami, S, and Ohno, N (1980). “A Continuum Theory of Creep and Creep Damage” *Creep in Structures*, 3rd IUTAM Symposium; Leicester; England, pp. 422-444.

[4] Hyde, T. H., Becker, A. A., and Sun, W. (2001). “Creep Damage Analysis of Short Cracks Using Narrow Notch Specimen made from a Ni-base Superalloy at 700°C” 10th International Conference on Fracture (ICF10), Hawai’i.

[5] Altenbach, J., Altenbach, H., and Naumenko, K. (2004). “Edge Effects in Moderately Think Plates under Creep-Damage Conditions” *Technische Mechanik*, 24(3-4): 254-263.

[6] Evans, R. W., Parker, J. D., and Wilshire, B. (1982). “An Extrapolative Procedure for Long Term Creep-Strain and Creep Life Prediction” Recent Advances on Creep and Fracture of Engineering Materials and Structures, Pineridge Press, pp. 135-184

[7] Ibanez, A. R., Srinivasan, V. S., Saxena, A. (2006). “Creep deformation and rupture behaviour of directionally solidified GTD 111 superalloy” *Fatigue and Fracture of Engineering Materials and Structures*, 29: 1010–1020.

[8] Gordon, A. P. (2006) “Crack Initiation Modeling of a Directionally-Solidified Ni-base Superalloy” PhD Thesis, Georgia Institute of Technology, Atlanta, GA.

[9] ASTM E-139. "Standard Test Methods for Conducting Creep, Creep-Rupture, and Stress-Rupture Tests of Metallic Materials” Vol. 03.01. West Conshohocken, PA.

[10] Cook, R.H. (1984). “Creep properties of Inconel-617 in air and helium at 800 to 1000°C” *Nuclear Technology*, 66(2): 283-288.

[11] Laanemae, W.M., Bothe, K., and Gerold, V. (1989) “High temperature mechanical behaviour of Alloy 617. 2. Lifetime and damage mechanisms” *Zeitschrift fur Metallkunde*, 80(12): 847-857.

[12] Larson, F. R., and Miller, J., (1952). “Time-temperature relationship for rupture and creep stresses” *American Society of Mechanical Engineers – Transactions*, 74(5): 765-771.
[13] Harada, H., Yamazaki, M., Koizumi, Y., Sakuma, N., Furuya, N. and Kamiya, H. (1982). "Alloy Design for Nickel-base Superalloys." *High Temperature Alloys for Gas Turbines*. F. Julich, Ed., Liege, Belgium, D. Reidel Publishing Co., pp.
[14] Kim, T. K., Yu, J. and Jeon, J. Y. (1992). "Creep rupture in a nickel-based superalloy." *Metallurgical Transactions A*, Vol. 23, No. 9, pp. 2581-2587.
[15] Srinivas, S., Pandey, M. C. and Taplin, D. M. R. (1995). "Air-Environment-Creep Interaction in a Nickel Base Superalloy." *Engineering Failure Analysis*, Vol. 2, No. 3, pp. 191-196.
[16] Ai, S. H., Xia, Y. B. and Tian, J. F. (1998). "The Creep and Fracture Behavior of Two Nickel-Based Superalloys." *Acta Metallurgica Sinica*, Vol. 11, No. 6, pp. 425-428.
[17] Sajjadi, S. A., Nategh, S., Isac, M. and Zebarjad, S. M. (2004). "Tensile deformation mechanisms at different temperatures in the Ni-base superalloy GTD-111." *Journal of Materials Processing Technology*, Vol. 155-156, No. 30, pp. 1900-1904.
[18] Ohno, N., T. Mizuno, Kawaji, H. and Okada, I. (1992). "Multiaxial creep of a nickel-base directionally solidified alloy: anisotropy and simulation." *Acta Metallurgica et Materialia*, Vol. 40, No. 3, pp. 559-567.
[19] Woodford, D. A. (1997). "Creep Analysis of Directionally-Solidified GTD111 based on Stress Relaxation Testing." *Materials at High Temperature*, Vol. 14, No. 4, pp. 413-420.
[20] Ibanez, A. R. (2003). "Modeling Creep Behavior in a Directionally Solidified Nickel Base Superalloy." Ph.D. Thesis, Georgia Institute of Technology, Atlanta, GA.